ADVANCED MATERIALS INTERFACES
Open Access
www.advmatinterfaces.de

Direct Evidence of the Presence of Hybrid Charge Transfer State in a Perovskite Nanocrystal-Polythiophene Blend Solid State Film

Tersilla Virgili, Mariacecilia Pasini, Michele Guizzardi, Edoardo Mosconi, Stefania Milanese, Luca Gregori, Asma A. Alothman, Maria Luisa De Giorgi, Arianna Creti, Maryna Bodnarchuk, Mauro Lomascolo, and Marco Anni**

In this paper, the photophysical properties of a hybrid material, composed of a conjugated polymer and perovskite nanocrystals, are investigated by ultrafast spectroscopy and morphological characterization. The relaxation dynamics of a drop-casted film from the semiconducting polythiophene (P3HT) and a green-emitting $CsPbBr_3$ (zwitterionic sulfobetaine -capped) perovskite nanocrystals (NCs) solution is studied. The transient spectroscopy presents a very long photobleaching signal peaked at 516 nm not present in the single components of the blend. The scanning electron and confocal fluorescence microscopy images show that the P3HT and the $CsPbBr_3$ NCs are finely mixed in the film. The presence of a very efficient hole transfer from the nanocrystal to the polymeric chain that induces the formation of a long -lived charge-transfer state as shown in the pump-probe measurements is proposed. The theoretical model reveals the important role of the zwitterionic sulfobetaine capper in this process. The perovskite strongly adsorbs the surfactant, while the polythiophene chain is not directly bound to the perovskite. Instead, it interacts with the surfactant itself, contributing to the electronic properties of the overall system.

1. Introduction

In recent years, metal halide perovskite semiconductors have demonstrated their exceptional capabilities in the optoelectronic field. This can be ascribed to their outstanding intrinsic photoelectric properties, such as high light harvesting abilities, long and balanced carrier diffusion lengths, high defect tolerance, high photoluminescence quantum yields, and readily tunable bandgaps.[1] The solution-processible, flexible, and cost-effective features make perovskite semiconductors even more appealing to the industry community. After decades of investigation, perovskites have been employed as active material in various fields, including solar cells, light-emitting diodes (LEDs), photodetectors, and lasers.[2] Despite these interesting features, the lack of long-term operational

T. Virgili
Istituto di Fotonica e Nanotecnologie – Consiglio Nazionale delle Ricerche (CNR)
Piazza Leonardo da Vinci 32, Milano 20133, Italy
E-mail: tersilla.virgili@cnr.it

M. Pasini
Istituto di Scienze e Tecnologie Chimiche "Giulio Natta"— SCITEC—CNR
via Corti 12, Milano 20133, Italy

M. Guizzardi
Dipartimento di Fisica
Politecnico di Milano
Piazza Leonardo da Vinci 32, Milano 20133, Italy

The ORCID identification number(s) for the author(s) of this article can be found under https://doi.org/10.1002/admi.202401004

DOI: 10.1002/admi.202401004

E. Mosconi
Computational Laboratory for Hybrid and Organic Photovoltaics – Istituto CNR di Scienze e Tecnologie Chimiche
SCITEC-CNR
Via Elce di Sotto 8, Perugia 06123, Italy

E. Mosconi, A. A. Alothman
Chemistry Department
College of science
King Saud University
Riyadh 11451, Saudi Arabia

S. Milanese, M. L. De Giorgi, M. Anni
Dipartimento di Matematica e Fisica " Ennio De Giorgi"
Università del Salento
Via per Arnesano, Lecce 73100, Italy
E-mail: Marco.anni@unisalento.it

L. Gregori
Department of Chemistry, Biology and Biotecnology
University of Perugia and INSTM
Via Elce di Sotto 8, Perugia 06123, Italy

stability to date still prevents the use of lead halide perovskites in general, and of their nanocrystals [NCs] in particular, in commercially available devices. In particular, the two main degradation channels of perovskites NCs are related to the interaction with the environmental moisture and oxygen[3] and, in electrically driven devices, to ion migration under applied bias[4,5] The potential sources of these instabilities are numerous, ranging from inherent materials instabilities to the influence of device operation (e.g., ion migration, joule heating, etc.). In the case of the perovskite emitting layer itself, it has been demonstrated that the quasi-2D heterostructures[6] themselves can be catastrophic for stability. To overcome the instabilities of these quasi-2D heterostructures a comprehensive understanding of these structures, their energetic landscape, and the charge-carrier dynamics within/across them has been developed.[7] A particularly promising strategy to reduce these effects is the NCs inclusion within inert polymeric matrices.[8,9] Even more interesting is the possibility of blending perovskite NCs with semiconducting polymers, able to stabilize perovskites by improving film morphology and environmental stability.[10] Additionally, their electronic properties enable the creation of hybrid materials that combine the electrical and optical characteristics of both components. This results in active properties that are unattainable with individual materials, allowing the generation of hybrid composites that merge the electrical and optical properties of both components.[11]

E.g., blends between blue emitting NCs and orange emitting poly[2-methoxy-5-(2-ethylhexyloxy)-1,4-phenylenevinylene] (MEH:PPV) have been used as active films in LEDs[12] showing an emission spectrum made by the superposition of the component materials ones and an emission color controllable by acting on the blend relative content. The emission color tunability and lasing activities of hybrid polymer–NCs blends have been later investigated in detail[13,14] using red or green emitting NCs blended with Polyfluorenes derivates. Despite these promising results, the details of the interaction processes between the organic and the perovskite components of the hybrid blends are still unclear. Most of the time, Forster Resonant Energy Transfer (FRET) from the polymer to the NCs or vice versa is claimed, only taking into account the spectral overlap between the host photoluminescence and the guest absorption.[14–17] A recent investigation of the PL relaxation dynamics indicated that FRET is not the main interaction process, instead suggesting the presence of bidirectional charge transfer between the polymer and the NCs.[11,13]

A. Creti, M. Bodnarchuk, M. Lomascolo
CNR-IMM
Institute for Microelectronic and Microsystems Unit of Lecce
Via per Monteroni, Lecce 73100, Italy
M. Bodnarchuk, M. Lomascolo
Laboratory for Thin Films and Photovoltaics
Empa – Swiss Federal Laboratories for Materials Science and Technology
Überlandstrasse 129, Dübendorf CH-8600, Switzerland
M. Bodnarchuk, M. Lomascolo
Institute of Inorganic Chemistry
Department of Chemistry and Applied Bioscience
ETH Zürich
Vladimir Prelog Weg 1, Zürich CH-8093, Switzerland

The lack of a clear understanding of the kind of interaction between the polymer and the NCs in the blend is currently a strong limit in the understanding of the potential of the use of those hybrid (organic-inorganic) blends in photonic and optoelectronic devices. E.g., to address unbalanced charge transport within perovskite photoactive layers, different groups report perovskite solar cells with a bulk heterojunction device structure, where solution-processed perovskites were mixed with the n-type electron acceptors, such as fullerene derivatives and low optical gap conjugated organic molecules.[18–20]

In this paper, we explore by ultrafast spectroscopy, morphological characterizations, and computational theory the photophysical properties of a drop-casted film from a polythiophene and green-emitting $CsPbBr_3$ (zwitterionic sulfobetaine -capped) nanocrystals solution. The transient spectroscopy shows a very long photobleaching signal peaked at 516 nm not present in the single components of the blend which we attribute to a charge transfer state formed in the interface between the NC and the polymeric chain. The computational model shows the role of the zwitterionic sulfobetaine surfactant in this interaction. Our results provide a strong evidence of the interaction between an active polymer and perovskite NCs blends and are expected to be relevant for the development of photoelectric devices, like solar cells, and photodetectors based on hybrid blends.

2. Results and Discussion

As the active materials in our experiments, we have used a P3HT:$CsPbBr_3$ film, drop casted from a solution with relative concentration 1:1 in weight. The normalized absorption and photoluminescence spectra of the single components and of the blend are shown in **Figure 1**.

The absorption peak of the NCs film is dominated by an excitonic peak at 500 nm, with a long tail due to scattering at higher wavelengths, while the P3HT and the blend films have a broad absorption band with peaks at ≈600 nm (2.07 eV, $A_{0\text{-}0}$), 546 nm (2.25 eV, $A_{0\text{–}1}$), and 510 nm (2.43 eV, $A_{0\text{–}2}$) that reflect the transition from the lowest vibrational level of the ground state to different vibrational levels of the excited-state manifold (the subscript referring to the number of vibrational quanta ν in the initial/final states, with $\nu = 0, 1, 2, \ldots$), evidencing that the C = C symmetric stretch at 0.18 eV dominates the coupling with the electronic states.[21] In the blend the contribution from the polymer completely hides the one from the NCs, probably due to a higher transition cross-section of the excitonic peak.

Figure 1b shows the PL spectra for the three samples. The NCs show a narrow emission band (100meV) peaked at 518 nm. Based on single NC spectroscopy[22] and 2D electronic (2DE) spectroscopy,[23] the heterogeneous line width is expected to be ≈25 meV, then the remaining line width should arise from electron–phonon coupling. The emission from the polymeric film presents two main peaks at 712 nm (1.74 eV) and 790 nm (1.57 eV), ascribed to the 0-0 and 0–1 transitions. The blend PL spectrum can be almost considered as the sum of the separated contributions from the two components; however, while in the absorption spectra, the contribution from the polymer dominates, in the PL the main contribution is given by the NCs, likely due to the higher PL quantum yield of the NCs with respect to the P3HT.[24,25]

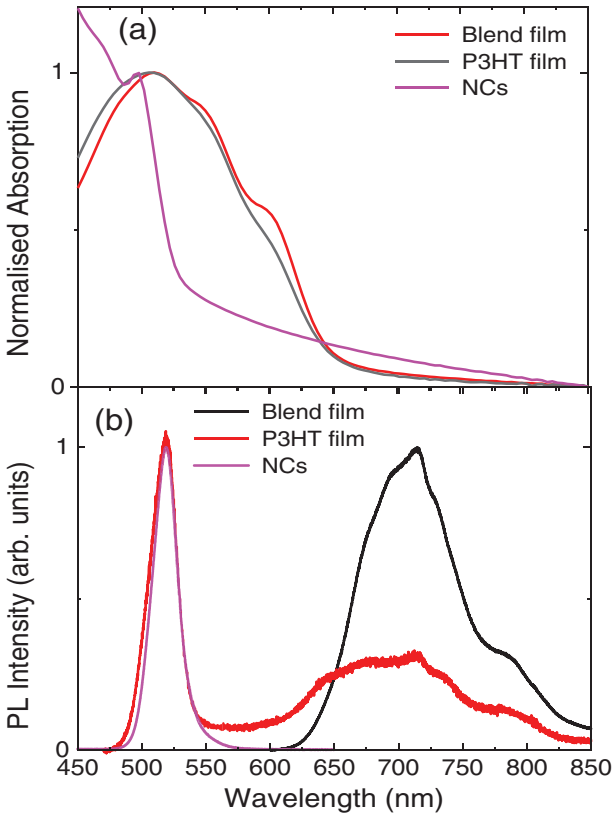

Figure 1. a) Normalized absorption spectra of the P3HT (black line), blend film (red line), and NCs (magenta lines). b) Normalized photoluminescence spectra after 405 nm pump excitation. Same line colors of (a).

To explore a possible interaction between the polymer and the NCs, we have performed ultrafast pump probe spectroscopy on both the NCs, the polymer and the blend drop cast films. All measurements on films are discussed in terms of the fractional change in the transmitted probe signal pulses at 2 kHz and probed with time-delayed broadband white light pulses at 1 kHz. Further details can be found in the Experimental Section.

$$\Delta T/T(t) = (T_{ON}(t) - T_{OFF})/T_{OFF} \quad (1)$$

where $T_{ON}(t)$ and T_{OFF} are the transmitted (T) probe signal with and without the optical pump, respectively, and t is the pump-probe delay. All samples were pumped at 400 nm using 100 fs pulses.

Figure 2a shows the pump probe spectra at 225 fs, 1 ps, and 3 ps probe delay for the NCs solid state film. The spectra reveal three different peaks at 475, 500, and 516 nm. They have different behaviors in time (see Figure 2b). The initial pump excitation induces an instantaneous bleaching signal at 475 nm and a photoinduced absorption one at 516 nm, while the bleaching signal at 500 nm presents a 1 ps raising time. After 1 ps both the signals at 475 nm and at 516 nm change sign. This process can be understood as a carrier relaxation within the band edge manifold after the initial pump excitation, a first step in the cascade of processes in light emission, as already reported by Strandell D. et al.[22]

Figure 3a shows the pump probe spectra at 250 fs, 3 ps, and 20 ps probe delay for the P3HT thin film. The transient absorption spectra of P3HT thin films have been extensively investigated.[26] In agreement with the previous assignment,[27] the positive bands at 510, 560, and 610 nm, are attributed to the photobleaching (PB) of the lowest vibronic resonances of the ground state (see Figure 3b) while the negative PA band at ≈660 nm, instead, is commonly attributed to instantaneously photogenerated polaron pairs.[28]

Figure 4a shows the pump probe spectra at different probe delays for the blend film. The spectra clearly show four positive bands peaked at 500, 516, 560, and 610 nm and a negative band at 480 nm. Looking at the comparison with the single components after 1 ps and 400 ps (see Figure 4b,c), we can assign the peaks at 480 nm and at 500 nm mainly to the NCs (even if the peak at 500 nm is slightly red shifted by 2 nm due to the overlapping P3HT absorption bleaching, that increases with the wavelength in this spectral range) while the two broad bands at 560 nm and at 610 nm to the polymer. The peak at 516 nm instead cannot be ascribed to any of the individual materials. Actually, in the NCs spectrum (blue line in Figure 4b), a very small signal is observed at 516 nm, that is positive only for ≈50 ps after photoexcitation (see blue line Figure 4f), while the 516 nm peak in the blend spectrum is always positive and it is much stronger. Looking at the P3HT spectrum (red line in Figure 4b) a positive bleaching band is present with a peak at ≈510 nm. However, the 516 nm bleaching peak in the blend spectrum is much narrower than the one of the P3HT and its intensity is three times higher than the one expected from the polymer (see red line Figure 4b). In addition, the relaxation dynamic of the 516 nm bleaching peak of the blend is much slower than the one of the P3HT. Overall these features evidence that the 516 nm peak in the blend does not come from NCs and P3HT, and it can be ascribed to an effect of the interaction between the NCs and the polymeric chain. The time decays of the main bands in the blend film are shown in Figure 4d, while the comparisons of the main bleaching band at 500 nm and the new one at 516 nm are shown respectively in Figure 4e,f. In the blend the decay of the main excitonic peak of the NC (at 500 nm) becomes faster (see black line in Figure 4e) than in the single component (blue line Figure 4e), while in Figure 4f the dynamic of the peak at 516 nm is much longer than the ones at the same wavelength in the polymeric or the NCs film.

To better understand the origin of the novel state observed in the hybrid film, we performed time-resolved PL measurements. The PL relaxation dynamics of the NCs (see Figure S1a, Supporting Information) can be reproduced by a tri-exponential decay, with lifetimes of $\tau_1 = 100 \pm 15$ ps, $\tau_2 = 650 \pm 20$ ps, and $\tau_3 = 7100 \pm 300$ ps. A qualitatively similar decay is observed for NCs in the hybrid film, but with lifetimes shortened down to $\tau_1 = 65 \pm 9$ ps, $\tau_2 = 380 \pm 50$ ps, and $\tau_3 = 1630 \pm 130$ ps, clearly evidencing the presence of a further relaxation channel in the blend film, consistent with the faster dynamics of the excitonic peak at 500 nm revealed in the pump-probe measurements.

Smaller variations are observed for P3HT (see Figure S1b, Supporting Information), showing a biexponential decay with lifetimes $\tau_1 = 10 \pm 1$ ps and $\tau_2 = 54 \pm 3$ ps, that becomes faster in the blends, with τ_1 decreasing to ≈1 ps, and τ_2 to 37 ± 1 ps.

We anyway observe that, despite the evidence of an additional decay channel for the NCs PL in the blend, no signatures of novel emitting states at higher wavelength of the NCs

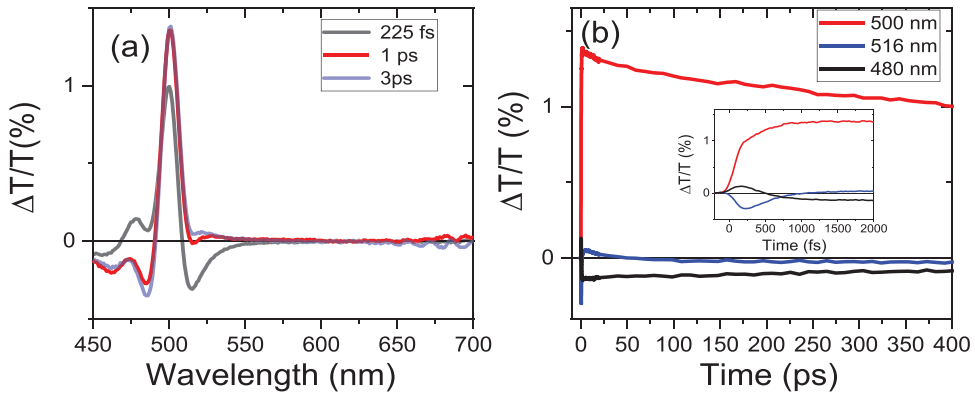

Figure 2. a) Pump probe spectra at different probe delays and b) time dynamics at different wavelengths for the NCs film. In the inset a zoom in the first 2 ps.

PL peak are found, either in the PL spectra at different time delays from the excitation pulse (see Figure S2a, Supporting Information) or in the PL relaxation dynamics (see Figure S2b, Supporting Information). We can thus conclude that the P3HT-NCs interaction does not lead to the formation of novel emitting states.

In order to further investigate the optical and structural properties of the blend film we evaluated the film morphology through confocal photoluminescence measurements to understand the spatial dispersion of the nanocrystals in the polymeric matrix. As shown in **Figure 5**, the P3HT emission is not uniform, showing the presence of brighter islands with a lateral size of ≈10 µm. In addition, bright green emitting clusters, with a lateral size of ≈1 µm are also visible, evidencing the presence of NCs clustering. We anyway observe that in the NCs clusters position also red emission of P3HT is present (see circles in Figure 5), demonstrating that no phase separation is present between the two components of the blend.

Further insight in the polymer and NCs distribution is provided by SEM measurements, clearly showing, at low magnification, that the regions with brighter P3HT emission are islands with locally higher thickness and the regions with strong NCs PL are actually NCs clusters. At higher magnification, the presence of smaller NCs clusters embedded within the polymer can be observed, allowing to conclude that the two components of the blend are finely mixed in the hybrid film.

Overall, both the pump-probe and the time-resolved PL measurements evidence the presence of a further decay process in the blend, mainly affecting the relaxation dynamics of the NCs and leading to the formation of a novel long lived absorbing, but not emitting, state.

To gain insight into the structural and electronic properties of the P3HT/NCs blend, we performed DFT simulations. As the first step, we move to analyze the nature of the interfaces considering the components of the blend and how they interact. We simulate all the possible interfaces present in the heterojunction: perovskite and polymer, perovskite and surfactants, polymer and surfactants. To have a wide overview of the structure and energetics of the interfaces, we also explored an alternative polymer and two different surfactants. As an alternative polymer, we simulated the polyfluorene (PFO) since it was experimentally found not to show the long living state provided by the P3HT based blend (see Figure S3, Supporting Information), while for the alternative ligands, we analyzed the oleic acid (OAc) and the oleylammine (OAm) recently used for the functionalization of $CsPbBr_3$ NCs for photonic applications.[29] In **Figure 6**a–c we report the optimized structures of the investigated ligand/perovskite interfaces. Concerning the surfactant passivation structure, we can

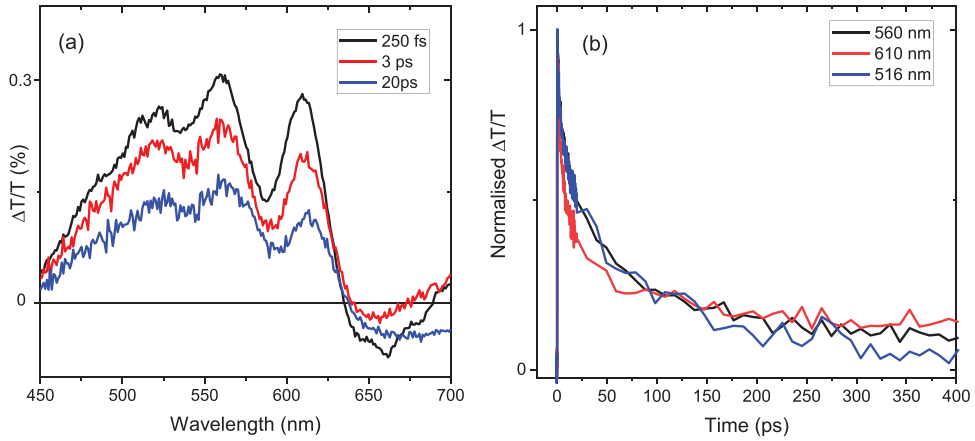

Figure 3. a) Pump probe spectra at different probe delays and b) time dynamics at different wavelengths for the P3HT film.

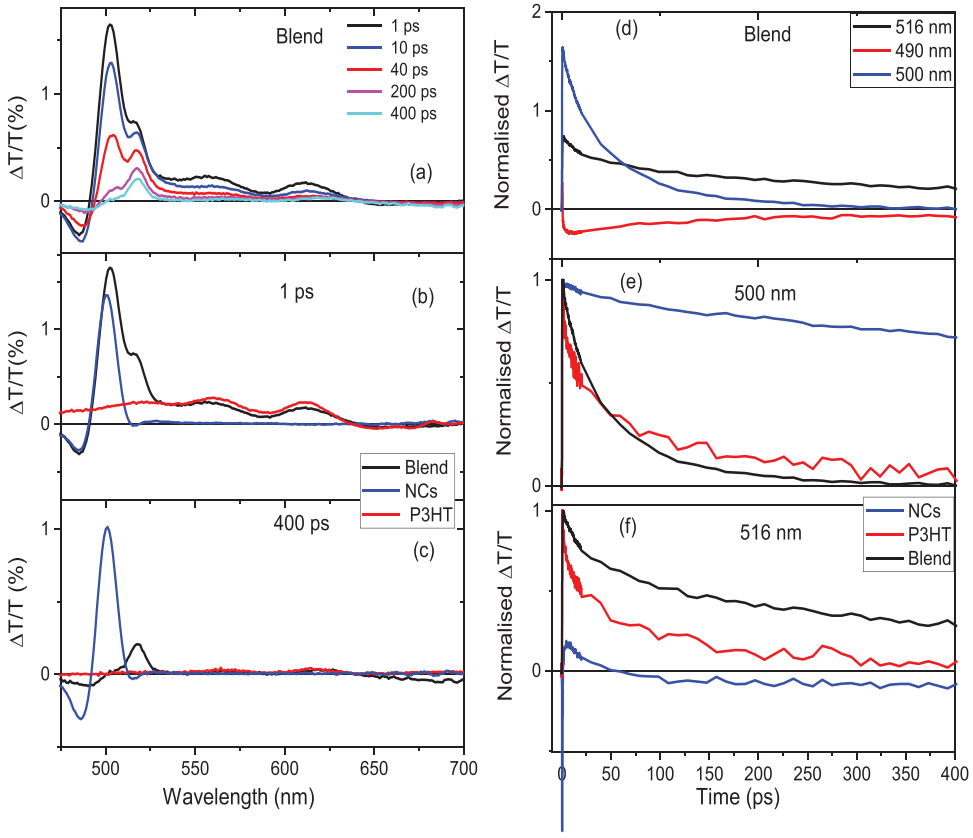

Figure 4. a) Pump probe spectra at different probe delays for the blend; b) Pump probe spectrum at 1 ps probe delay for the blend (black line), the NCs (blue line), and the P3HT (red line) film; c) Pump probe spectrum at 400 ps probe delay for the blend (black line), the NCs (blue line), and the P3HT (red line) film; d) Time dynamics at different wavelengths for the blend; e) Time dynamic at 500 nm and f) at 516 nm for the blend (black line), the NCs (blue line), and the P3HT (red line) film.

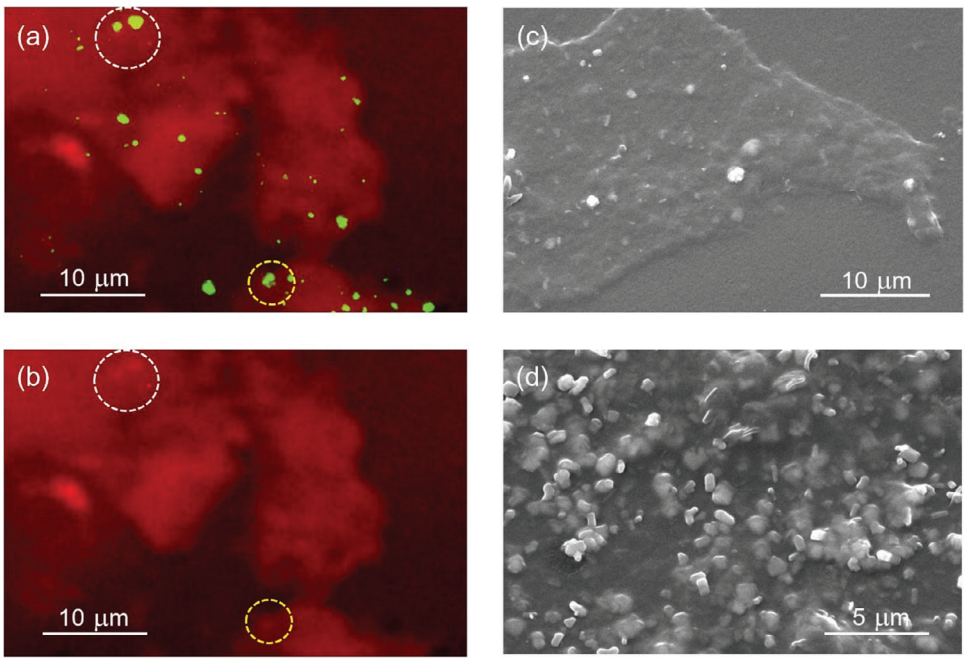

Figure 5. Confocal photoluminescence maps of the blend film (a,b). a) The red emission is from the polymer and the green one from the NC. (b) Confocal photoluminescence map at the P3HT emission wavelength. The circular spots are placed to indicate the same spatial spot in the two images. SEM images of the SEM film at c) 3000x and d) 5000x magnification.

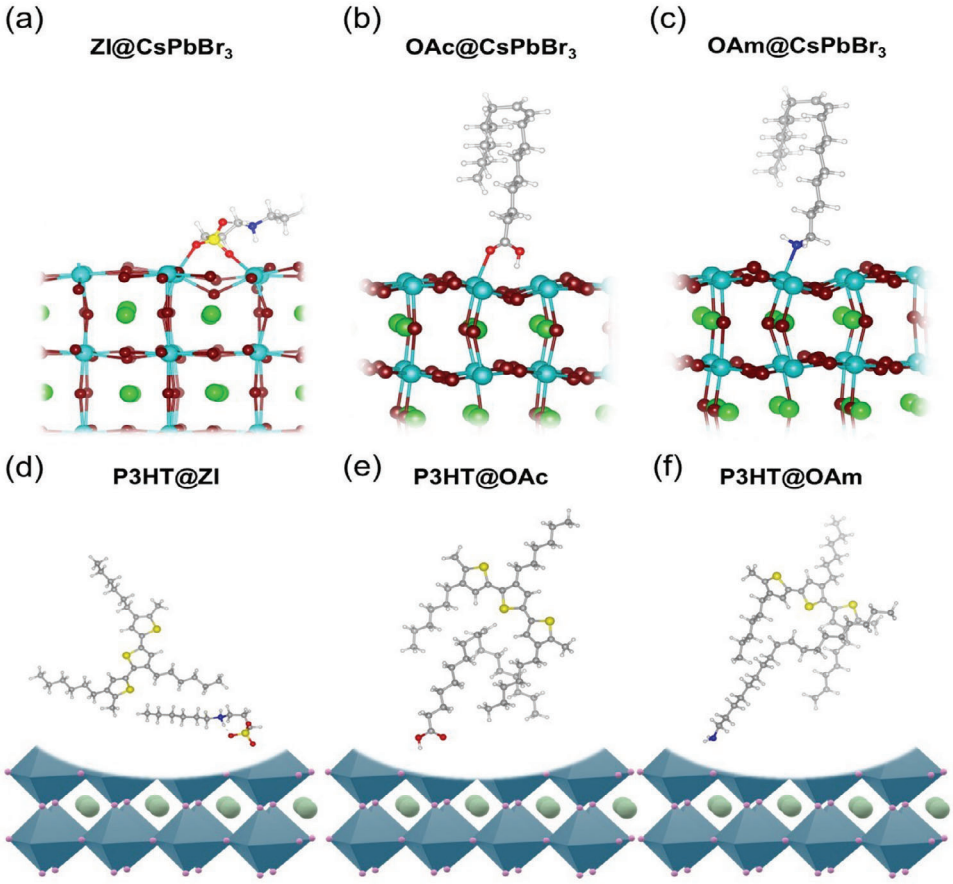

Figure 6. Perovskite/ligand and P3HT/ligand interfaces for a,d) ZI, b,e) OAc, c,f) OAm.

clearly observe that the ZI is flat while the OAc and OAm are more perpendicular with respect to the perovskite surface. The adsorption energies (E_{ads}) reported in **Table 1** clearly indicate that the ZI gives a more stable perovskite passivation layer with respect to the other ligands because of the nature of its interaction. In particular, ZI is adsorbed through two oxygen of the $-SO_3^-$ group and an additional hydrogen bond of the ammonium group toward an Br atom that induces the molecule to be flat on the surface. On the other hand, OAc and OAm show more perpendicular orientation and are interacting only by one anchoring atom, O and N respectively. Moreover, by comparing the ZI and polymers adsorption energies, we noticed that also in this case the surfactant provides the highest interaction energy confirming the expected heterointerface: the perovskite NC is passivated by the ligands (ZI) and then surrounded by the polymer. Having established the perovskite/ligand interface structure we move to simulate how the polymers interact with the ligand passivating layer. We prepare the ligand/P3HT interacting model considering the ligand fixed with the anchoring group to the geometry optimized on the perovskite surface. We simulated the P3HT polymer as a

Table 1. Calculate band gap (Eg), adsorption and interaction energies (E_{ads} and E_{int}) and valance band shift (ΔVB).

	E_g, eV	E_{ads} (E_{int}), eV	ΔVB, eV
$CsPbBr_3$	2.09	–	0.0
P3HT@$CsPbBr_3$	1.99	0.92	+ 0.19
PFO@$CsPbBr_3$	2.07	1.06	+ 0.44
ZI@$CsPbBr_3$	2.09	3.18	+ 0.51
OAc@$CsPbBr_3$	2.08	0.78	+ 0.24
OAm@$CsPbBr_3$	2.04	0.94	+ 0.35
P3HT@ZI	–	0.71	–
P3HT@OAc	–	0.79	–
P3HT@OAm	–	0.77	–

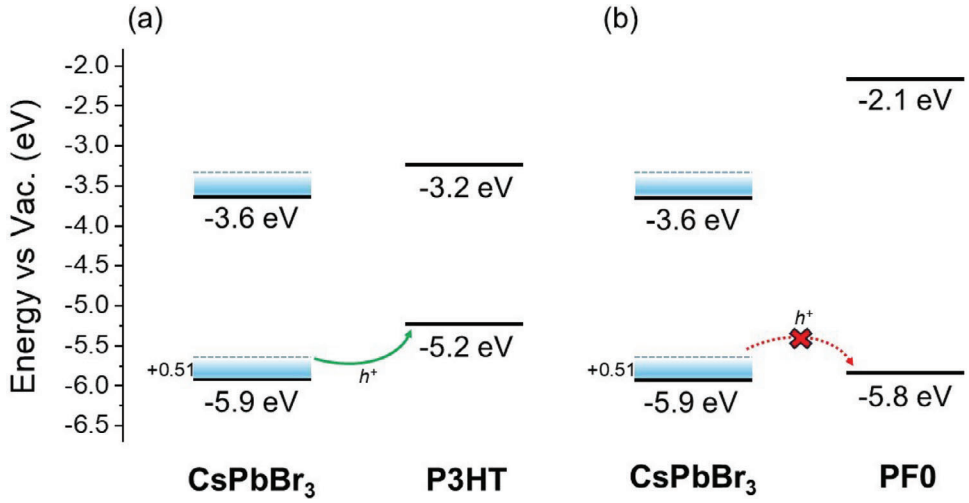

Scheme 1. Schematic representation of the energy levels alignment between perovskite and investigate polymers: a) P3HT, b) PFO. The blue dashed lines indicate the expected upshift of the levels induced by the ZI perovskite passivation.

trimer that is long enough to interact with the whole molecule, see Figure 6d–f.

This simplified approach allows us to have an indication on the interacting energy (E_{int}) and on the distance between the polymer and the hypothetic perovskite surface. As a matter of fact, while the ligand/P3HT E_{int} of ZI, OAc and OAm are similar, see Table 1, the geometries appear quite different with the ZI that, thanks to its flat adsorption rearrangement, permit the P3HT to be placed closer to the perovskite surface with respect to the other ligands. This, in principle, would lead to more efficient charge transfer in the blend upon photoexcitation.

Verified the nature of the blend in terms of structure and interfaces, we move to evaluate the possibility of charge transfer from the perovskite to the polymer under light exposure to justify the experimental measurements reported above.

In principle, to permit a proper charge transfer, a good energy level alignment is required. Concerning the energy level versus vacuum of the P3HT polymer, it is shown to have a VB level ≈ − 5.2 eV and a CB level ≈ − 3.2 eV[30] with a band gap ≈2.0/2.1 eV in line with the measurements here reported. Moving to the CsPbBr3, the scenario is more complex, and a variability is found in the literature by moving from powder, film, NC and Quantum Dot (QD). This is due to the size effect on quantum confinement and the effect of the morphology on the optical behavior. E.g., film CsPbBr3 shows a VB ≈ − 5.6 eV,[31] for the NC we can find VB values between ≈ − 5.9/ − 6.0 eV[32] and finally for QD we also have a VB of − 6.3 eV. Considering these data, the energy alignment between the P3HT and the CsPbBr3 NC would be similar to that reported in **Scheme 1**a, where we have the polymer VB and CB above to the respective perovskite levels in line with a type-II heterojunction.[33] This energy alignment was already found for a similar system for photovoltaic applications[34] providing the hole transfer from the perovskite to the polymer. Interestingly, another important aspect that could tune the level of the ionization potential of the organo-halide lead perovskite, that can be approximated to the VB energy, is the role the surface treatment and passivation.[35] To consider this aspect we calculate the VB level, see Computational Section, by varying the ligand adsorbed onto per perovskite surface. As we can see in Table 1, we reported the calculated VB shift with respect to the bare perovskite and we noticed an important role of the ligand. In particular, all investigated ligands induce an upshift of the perovskite VB with the ZI that provide the highest effect (+0.51 eV). This upshift, even if important, does not lead to a different energy level alignment scheme maintaining the P3HT VB and CB level above the perovskite respective levels, and this in principle does not strongly affect the observed charge transfer. If this is expected for P3HT, the situation is very different for the PFO polymer. In fact, since PFO has a VB energy level of −5.8 eV and CB of −2.1 eV,[36] this provides a non-proper energy level alignment hindering the hole transfer and leading to a type-I heterojunction with a straddling gap[33] where perovskite VB and CB edges are entirely within the bandgap of the PFO polymer, see Scheme 1b. While the type-I heterojunction, such as PFO/$CsPbBr_3$, is affected by charge recombination processes due to lack of an efficient charge separation, type-II heterojunction, such as P3HT/$CsPbBr_3$, shows important advantages as a good charge separation, reduction of recombination processes and increase of charge transfer efficiency. By considering this different energy alignment type in Scheme 1, both the heterojunctions (P3HT/$CsPbBr_3$ and PFO/$CsPbBr_3$) provide the possibility of electron injection from the polymer CB to perovskite CB upon polymer photoexcitation. While this electron transfer could happen with both polymers, the hole transfer is permitted only in the P3HT case due to its favorable VB energy alignment with the perovskite VB. As a matter of fact, since PFO does not form an efficient heterointerface with $CsPbBr_3$ in terms of charge separation, it is not able to accept hole from the $CsPbBr_3$ VB and it does not provide the peaks at 516 nm in the pump probe spectra (see Figure S3, Supporting Information); In the P3HT/$CsPbBr_3$ heterojunction, we could assign this signal to the hole transfer from the perovskite to the polymer.

The DFT simulations helped us to understand the nature of the new absorptive state at 516 nm present in the blend. We think that this transition is due to a hybrid charge transfer state formed at the interface between the NC and the polymeric chain.

Other works reported charge transfer in the solution of colloidal CsPbBr3 perovskite nanocrystals by heterovalent doping.[37] In contrast, our study investigates the interaction in a solid-state system composed of a $CsPbBr_3$-ZI P3HT film deposited by drop-casting. We employ an organic polymer, and, in comparison with the approach of Raihana Begum et al.,[37] this cannot be considered doping, as the polymer remains in a neutral state.

3. Conclusions

In this paper, we exploited by ultrafast spectroscopy, morphological characterizations, and computational theory the photophysical properties of a drop casted film from a polythiophene and green-emitting $CsPbBr_3$ (zwitterionic sulfobetaine-capped) nanocrystals solution. We showed by transient spectroscopy the presence of a long-lived absorptive state present in the blend drop cast film by computational analysis, and we attributed this state to a charge transfer state originated by a hole transfer from the NC and the polymeric chain with the help of the zwitterionic sulfobetaine surfactant. Our results provide a strong evidence of the interaction between an active polymer and perovskite NCs and are expected to be relevant for the development of photoelectric devices, like solar cells and photodetectors based on hybrid blends.

4. Experimental Section

Nanocrystal Synthesis and Film Preparation: The synthesis of $CsPbBr_3$ NCs was performed following ref. [38] with modifications detailed below. Trioctylphosphine-Br_2 precursor was injected into a mixture of lead oleate and zwitterionic ligand ASC18 (3-N,N-(dimethyloctadecylammonio)propanesulfonate) in octadecene at 135 °C under a nitrogen atmosphere. The reaction was rapidly quenched within 10 s using an ice bath.

Subsequent purification and size-selection steps were performed in a glovebox under inert conditions using anhydrous solvents. First, the crude solution was centrifuged at 29 500 g for 10 min. The precipitate was discarded and 40 mL of anhydrous ethyl acetate was added to the supernatant, followed by centrifugation at 29 500 g for 5 min. The precipitate was discarded, and 10 mL of anhydrous ethyl acetate was added again to the supernatant, followed by centrifugation at 29 500 g for 5 min. The obtained precipitate was dissolved in 2 mL of anhydrous toluene, and the supernatant was discarded. The final colloid had a concentration of ≈16 mg mL^{-1} and was used for further studies.

The samples were prepared by blending P3HT (≈93% RegioRegular, with number-average molecular weight (M_n) in the 15–45 kDa range, Sigma-Aldrich) and $CsPbBr_3$ nanocrystals. These were dispersed into toluene solutions with a concentration of 1.7 mg mL^{-1} and then drop casted onto a quartz substrate. To achieve the blend solution, an identical amount of the individual solution was mixed in the same vial to achieve a 1:1 blend in weight.

Continuous Wave and Time Resolved Photoluminescence: The photoluminescence (PL) spectra under continuous wave excitation were measured by exciting the film with a 405 nm laser diode. The PL was dispersed by an Acton Research Corporation Spectra Pro-750 spectrometer and detected by a Peltier cooled CCD (Andor).

Time-resolved PL was excited by a 20 fs pulse delivered at 75 MHz repetition rate from the second harmonic 400 nm line of a Ti: sapphire laser (10 mW), in conjunction with a streak camera (C10910-05 Hamamatsu). The time resolution of this setup was ≈1ps.

Microscopy: The local investigation of the film PL properties was performed by Laser Scanning Confocal Microscopy with a Nikon Eclipse C1 inverted confocal microscope using a 40X dry objective. The samples were excited by the 405 nm line of a diode laser and the PL signal was detected by a photomultiplier in the 530 ± 20 nm and 705 ± 15 nm spectral range, for the NCs and P3HT, respectively.

The local morphology was also investigated by means of a Scanning Electron Microscope (JEOL JSM-6480LV) operating at an accelerating voltage of 10 kV. In order to prevent charging effects, the samples were previously metalized with gold by means of sputtering deposition in argon (at a pressure of 1 × 10 − 1 mbar) (Quorumm Technologies – EMITECH K550X Sputter Coater), leading to a gold thickness of ≈10 nm.

Absorption: The absorbance spectra were measured with a Varian Cary 50 double beams spectrophotometer.

Pump and Probe Measurements: The ultrafast spectroscopy setup was fed by a 150 fs, 2 kHz repetition rate Ti:sapphire system (Libra, Coherent, Santa Clara, CA, USA) with a central wavelength of 800 nm. Transient-absorption measurements were performed by pumping at 400 nm (Power 15 µW) with the second harmonic of the laser output, generated with a 1 mm, Type I β-barium borate crystal. The probe pulses, with a spectrum spanning from 450 to 750 nm, were obtained by white-light generation in a 3 mm thick sapphire crystal. The measurements were performed in transmission, and the probe spectrum was detected using a SP2150 Acton, Princeton Instruments spectrometer. The pump beam was modulated by a mechanical chopper at a 1 kHz frequency, and the differential transmission ($\Delta T/T$) spectrum of the probe was measured as a function of probe wavelength and pump–probe delay. The polarization between the pump and probe beams was set at magic angle (54.7°).

Theoretical Model: DFT calculations were carried out on the (001) CsPbBr3 surface within the supercell approach using the Perdew-Burke-Ernzerhof (PBE) functional.[39] The plate consists of a 2 × 2 tetragonal supercell in the a and b periodic directions and five layers along the perpendicular non-periodic direction, with a 15 Å region of vacuum added in all cases. Starting from the flat PbBr2 terminated (001) surface, different adsorption systems were studied. The total adsorption energy (EAds) is calculated following this equation:

$$EAds = [Epass - slab - (Epristine - pass)] \quad (2)$$

where Epass-slab is the total energy of the passivated slab; Epristine is the total energy of the pristine PbI2 terminated bare surface and pass is the energy of the isolated molecule. EAds were normalized by dividing by the number of site (n) corresponding to the number of undercoordinated Pb atoms on the two surfaces. Dispersion interactions are considered on the optimized geometries using the D3 approach of Grimme.[40] The molecular geometries were optimized using 20 × 20 × 20 Å supercells, which are large enough to decouple long-range interactions. To calculate the interaction energy of each molecule, Gaussian implemented in the g09 software was used. The energy positions of the valence band maxima (VBM) on differently terminated surfaces were quantified by calculating the associated ionization energy (IE). The IE is defined here as the energy required to extract electrons from the valence band and is distinguished from the work function of the slab, which is the energy required to extract electrons from the Fermi level and is significantly influenced by carrier densities and surface defects. IEs were calculated by using the expression:

$$IE = E\,(vac) - E\,(VMB) \quad (3)$$

PBE surface calculations were performed by using norm-conserving pseudopotentials[41] (shells explicitly included in calculations: I 5s, 5p; N, C 2s, 2p; O 2s 2p; H 1s; Pb 6s, 6p, 5d) and a cutoff on the wavefunctions of 60 Ryd (240 Ryd on the charge density 1 × 1 × 1 k-points grid in the BZ). All calculations were performed by using the Quantum Espresso package.[42]

Supporting Information

Supporting Information is available from the Wiley Online Library or from the author.

Acknowledgements

The research has been partly financed by the Italian Ministry of University (MUR) under Contract P2022B3W29 (PRIN – PNRR 2022 – LOGIFIB) and financed by EU – Next Generation EU, Mission 4, Component 1, CUP: B53D23028440001 and by the EU – NextGeneration EU POR H2 – Mission 2, Component 2, CUPB93C22000630006. This work was partly funded by the Researchers Supporting Project number (RSP2025R243), King Saud University, Riyadh, Saudi Arabia. E.M. acknowledge funding from European Union's Horizon Europe research and innovation programme under grant agreement number 101082176 - VALHALLA.

Conflict of Interest

The authors declare no conflict of interest.

Data Availability Statement

The data that support the findings of this study are available from the corresponding author upon reasonable request.

Keywords

charge-transfer state, $CsPbBr_3$ nanocrystals, polythiophene, ultrafast spectroscopy

Received: December 17, 2024
Revised: January 31, 2025
Published online:

[1] M. R. Filip, G. E. Eperon, H. J. Snaith, F. Giustino, *Nat. Commun.* **2014**, *5*, 5757.
[2] L. Zhang, L. Mei, K. Wang, Y. Lv, S. Zhang, Y. Lian, X. Liu, Z. Ma, G. Xiao, Q. Liu, S. Zhai, S. Zhang, G. Liu, L. Yuan, B. Guo, Z. Chen, K. Wei, A. Liu, S. Yue, G. Niu, X. Pan, J. Sun, Y. Hua, W.-Q. Wu, D. Di, B. Zhao, J. Tian, Z. Wang, Y. Yang, L. Chu, et al., *Nano-Micro Lett.* **2023**, *15*, 177.
[3] M. L. De Giorgi, F. Krieg, M. V. Kovalenko, M. Anni, *Sci. Rep.* **2019**, *9*, 17964.
[4] W. Tress, *J. Phys. Chem. Lett.* **2017**, *8*, 3106.
[5] X. Shan, J. Li, M. Chen, T. Geske, S. G. R. Bade, Z. Yu, *J. Phys. Chem. Lett.* **2017**, *8*, 2412.
[6] H. Wang, Y. Chen, D. Li, *Int. J. Extrem. Manuf.* **2023**, *5*, 012004.
[7] F. V. A. Camargo, T. Nagahara, S. Feldmann, J. M. Richter, R. H. Friend, G. Cerullo, F. Deschler, *Am. Chem. Soc.* **2020**, *142*, 777.
[8] S. N. Raja, Y. Bekenstein, M. A. Koc, S. Fischer, D. Zhang, L. Lin, R. O. Ritchie, P. Yang, A. P. Alivisatos, *ACS Appl. Mater. Interfaces* **2016**, *8*, 35523.
[9] T. Xuan, J. Huang, H. Liu, S. Lou, L. Cao, W. Gan, R.-S. Liu, J. Wang, *Chem. Mater.* **2019**, *31*, 1042.
[10] P. Zhou, T. Bu, S. Shi, L. Li, Y. Zhang, Z. Ku, Y. Peng, J. Zhong, Y. Cheng, F. Huang, *J. Mater. Chem. C* **2018**, *6*, 5733.
[11] A. Balena, A. Creti, M. Lomascolo, M. Anni, *RSC Adv.* **2021**, *11*, 33531.
[12] E.-P. Yao, Z. Yang, L. Meng, P. Sun, S. Dong, Y. Yang, *Adv. Mater.* **2017**, *29*, 1606859.
[13] A. Perulli, A. Balena, M. Fernandez, G. Nedelcu, A. Cretı, M. V. Kovalenko, M. L. M. Anni, *Appl. Phys. Lett.* **2018**, *112*, 171904.
[14] A. Mikosch, S. Ciftici, G. Tainter, R. Shivanna, B. Haehnle, F. Deschler, A. J. C. Kuehne, *Chem. Mater.* **2019**, *31*, 2590.
[15] E.-P. Yao, Z. Yang, L. Meng, P. Sun, S. Dong, Y. Yang, Y. Yang, *Adv. Mater.* **2017**, *29*, 1606859.
[16] B. A. Al-Asbahi, S. M. H. Qaid, A. S. Aldwayyan, *Polymers* **2020**, *12*, 444.
[17] S. M. Qaid, B. Al-Asbahi, H. M. Ghaithan, M. Al Salhi, A. S. Al Dwayyan, *J. Colloid Interface Sci.* **2020**, *563*, 426.
[18] L. Shen, T. Zhu, X. Zhang, K. Gong, H. Wang, X. Gong, *Nano Energy* **2022**, *93*, 106907.
[19] Z. Guan, Y. Li, P. Man, H. Tan, Q. Wei, J. Liu, M. Li, T. H. Ly, J. Yin, C.-S. Lee, *Adv. Mater.* **2024**, *36*, 2407406.
[20] K. Wang C Liu, P. Du, J. Zhengb, X. Gong, *Energy Environ. Sci.* **2015**, *8*, 1245.
[21] J. Clark, J. F. Chang, F. C. Spano, R. H. Friend, C. Silva, *Appl. Phys. Lett.* **2009**, *94*, 163306.
[22] D. Strandell, C. Sonnichsen, P. Kambhampati, *J. Phys. Chem. C* **2022**, *126*, 20505.
[23] H. Seiler, S. Palato, C. Sonnichsen, H. Baker, E. Socie, D. P. Strandell, P. Kambhampati, *Nat. Commun.* **2019**, *10*, 8.
[24] O. P. Dimitriev, *Nanoscale Res. Lett.* **2017**, *12*, 510.
[25] J. Piris, T. E. Dykstra, A. A. Bakulin, P. H. M. Van Loosdrecht, W. Knulst, M. Tuan Trinh, J. M. Schins, L. D. A. Siebbeles, *J. Phys. Chem. C* **2009**, *113*, 14500.
[26] A. Portone, L. Ganzer, F. Branchi, R. Ramos, M. J. Caldas, D. Pisignano, E. Molinari, G. Cerullo, L. Persano, D. Prezzi, T. Virgili, *Sci. Rep.* **2019**, *9*, 7370.
[27] R. Alex Marsh, J. M. Hodgkiss, S. Albert-Seifried, R. H. Friend, *Nano Lett.* **2010**, *10*, 923.
[28] J. Guo, H. Ohkita, H. Benten, S. Ito, *J. Am. Chem. Soc.* **2009**, *131*, 16869.
[29] A. Manoli, P. Papagiorgis, M. Sergides, C. Bernasconi, M. Athanasiou, S. Pozov, S. A. Choulis, M. I. Bodnarchuk, M. V. Kovalenko, A. Othonos, G. Itskos, *ACS Appl. Nano Mater.* **2021**, *4*, 5084.
[30] B. Thompson, J. Fréchet, *Angew. Chem.* **2008**, *47*, 58.
[31] S. Ullah, J. Wang, P. Yang, L. Liu, S.-E. Yang, T. Xia, H. Guo, Y. Chen, *Mater. Adv* **2021**, *2*, 646.
[32] F. Mei, D. Sun, S. Mei, J. Feng, Y. Zhou, J. Xu, X. Xiao, *Adv. Phys.: X* **2019**, *4*, 106907.
[33] J. X. Low, J. G. Yu, M. Jaroniec, S. Wageh, A. A. Al-Ghamdi, *Adv. Mater.* **2017**, *29*, 1601694.
[34] C. M. Pelicano, H. Yanagi, *J. Energy Chem.* **2018**, *27*, 455.
[35] D. Meggiolaro, E. Mosconi, A. H. Proppe, R. Quintero-Bermudez, S. O. Kelley, E. H. Sargent, F. De Angelis, *ACS Energy Lett.* **2019**, *4*, 2181.
[36] F. So, B. Krummacher, M. K. Mathai, D. Poplavskyy, S. A. Choulis, V. Choon, *J. Appl. Phys.* **2007**, *102*, 091101.
[37] R. Begum, M. R. Parida, A. L. Abdelhady, B. Murali, N. M. Alyami, G. H. Ahmed, M. Nejib Hedhili, O. M. Bakr, O. F. Mohammed, *J. Am. Chem. Soc.* **2017**, *139*, 731.
[38] F. Krieg, S. T. Ochsenbein, S. Yakunin, S. ten Brinck, P. Aellen, A. Süess, B. Clerc, D. Guggisberg, O. Nazarenko, Y. Shynkarenko, S. Kumar, C.-J. Shih, I. Infante, M. V. Kovalenko, *ACS Energy Lett.* **2018**, *3*, 641.
[39] M. Ernzerhof, G. E. Scuseria, *J. Chem. Phys.* **1999**, *110*, 5029.
[40] S. Grimme, J. Antony, S. Ehrlich, H. Krieg, *J. Chem. Phys.* **2010**, *132*, 154104.
[41] M. J. Van Setten, M. Giantomassi, E. Bousquet, M. J. Verstraete, D. R. Hamann, X. Gonze, G.-M. Rignanese, *Comput. Phys. Commun.* **2018**, *226*, 39.
[42] P. Giannozzi, S. Baroni, N. Bonini, M. Calandra, R. Car, C. Cavazzoni, D. Ceresoli, G. L. Chiarotti, M. Cococcioni, I. Dabo, A. D. Corso, S. de Gironcoli, S. Fabris, G. Fratesi, R. Gebauer, U. Gerstmann, C. Gougoussis, A. Kokalj, M. Lazzeri, L. Martin-Samos, N. Marzari, F. Mauri, R. Mazzarello, S. Paolini, A. Pasquarello, L. Paulatto, C. Sbraccia, S. Scandolo, G. Sclauzero, A. P. Seitsonen, et al., *J. Phys.: Condens. Matter* **2009**, *21*, 395502.